Extending the Boore and Abrahamson (2023) Modified Square-Root-Impedance Method for the Development of Site Amplifications Consistent with the Full-Resonance Approach to a Range of V_{S30} Values

Linda Al Atik[1] and David M. Boore*[2]

ABSTRACT

The square-root-impedance (SRI) method is commonly used to approximate the seismic site amplifications computed using the full-resonance (FR) method for gradient shear-wave velocity (V_S) profiles that are smoothly varying with depth. The SRI site amplifications have been observed to systematically underpredict the FR site amplifications by a ratio of FR/SRI amplifications around 1.05 to 1.3 across a wide frequency range (Boore, 2013). Recently, Boore and Abrahamson (2023; hereafter, BA23) related this difference in the SRI and FR methods to differences in the exponent η of the ratio of seismic impedances between the two methods. They proposed the implementation of a modified frequency-dependent η in the SRI method to improve its match to the FR site amplifications. This modified η was derived using only five V_S profiles. We investigate the performance of the BA23 η for a wide range of realistic gradient V_S profiles with V_{S30} ranging from 180 to 1500 m/s. These gradient V_S profiles are constructed using two power-law functions of depth and are constrained by the assigned V_{S30} value, the depth and velocity of the half-space, and depths to shear-wave velocity horizons of 1.0 and 2.5 km/s ($Z_{1.0}$ and $Z_{2.5}$) based on western United States sites. Despite observing a V_{S30} dependence of η, we find that the BA23 η generally works reasonably well for the range of V_S profiles analyzed. Using the V_{S30}-dependent η derived in this study results in improvements in matching the FR site amplification compared to using the BA23 η. These improvements are more pronounced for the soft-site conditions and become modest to negligible for the stiff site conditions.

KEY POINTS

- Modifying the exponent η of the square-root-impedance (SRI) method results in site amplifications that better match those calculated using the full-resonance (FR) method.
- The Boore and Abrahamson (2023) simple η adjustment derived with five V_S profiles approximates reasonably well the FR site amplifications for a wide range of V_S profiles.
- The use of a V_{S30}-dependent η could lead to an improvement of the SRI site amplifications for site conditions with V_{S30} less than 400 m/s. For stiffer site conditions, the improvement is observed to be modest for most cases analyzed.

Supplemental Material

INTRODUCTION

Amplifications of seismic waves traveling through a shear-wave velocity (V_S) profile are typically calculated using the square-root-impedance (SRI) method or the full-resonance (FR) method. The SRI method, sometimes referred to as the quarter-wavelength method, is widely used for V_S profiles that are smoothly varying with depth and without strong impedance

1. Linda Alatik Consulting, San Francisco, California, U.S.A., https://orcid.org/0000-0002-2979-8330 (LAA); 2. U.S. Geological Survey, Earthquake Science Center, Moffett Field, California, U.S.A., https://orcid.org/0000-0002-8605-9673 (DMB)

*Corresponding author: dboore@yahoo.com

Cite this article as Al Atik, L., and D. M. Boore (2024). Extending the Boore and Abrahamson (2023) Modified Square-Root-Impedance Method for the Development of Site Amplifications Consistent with the Full-Resonance Approach to a Range of V_{S30} Values, *Bull. Seismol. Soc. Am.* **XX**, 1–10, doi: 10.1785/0120240112

contrasts. Furthermore, the analytical solution provided by the SRI method allows for the inversion of average site amplifications in ground-motion prediction models (GMPMs) to develop GMPM-compatible V_S profiles (e.g., Al Atik and Abrahamson, 2021; Phung and Abrahamson, 2024). On the other hand, the FR method computes site amplifications that are based on theoretical simulations of wave propagation in layered profiles accounting for the constructive and destructive interference of all reverberations in the layers (Boore, 2013). As such, the FR method is well suited for site response analyses of the near-surface materials and for profiles with strong changes in impedance that can lead to resonance peaks in the site amplification.

Although the SRI method provides a fast way of computing reasonable approximations to site amplifications of V_S profiles that are not sensitive to the details of the profile, Boore (2013) evaluated the differences between the SRI and FR site amplifications for a range of V_S profiles and concluded that the SRI method consistently underestimates the FR response over a wide range of frequencies by up to 30% for gradient V_S profiles. Recently, BA23 related the difference between the SRI and FR amplifications for gradient profiles to the underlying features of the two methods: the FR amplifications are controlled by the ratio of seismic impedances, whereas the SRI amplifications are calculated based on the square root of the ratio of seismic impedances. To address this, BA23 proposed a relatively simple modification to the SRI amplifications to better match those obtained with the FR method. This proposed modification was based on the analysis of five generally stiff V_S profiles. Although this modification generally improves the agreement between the SRI and the FR site amplifications, the adjustment may not work equally well for a wide range of gradient V_S profiles.

In this article, we examine the SRI adjustments of BA23 and investigate their applicability to a large number of V_S profiles with varying site conditions. For this purpose, we sample a wide range of gradient V_S profiles with time-averaged shear-wave velocity over the top 30 m of the profile (V_{S30}) from 180 to 1500 m/s and develop SRI adjustments that are V_{S30} dependent. We then assess the improvement in site amplifications using the V_{S30}-dependent SRI adjustments compared to those obtained with the BA23 adjustments using the FR site amplifications as a benchmark. The article starts with a brief overview of the BA23 approach followed with a description of our methodology including the sampling of realistic V_S profiles. The results are then presented and discussed followed by the presentation of the V_{S30}-dependent SRI adjustments and the examination of the applicability of the BA23 adjustments to various site conditions in light of this study. We note that the accuracy of the FR method in approximating the true site amplification is beyond the scope of this study, which is to reduce the mismatch between the SRI and the FR site amplifications for gradient V_S profiles. As noted in Boore (2013), site amplifications from either method should be taken as approximations of the true 3D amplification.

OVERVIEW OF THE BA23 SRI MODIFICATION

The SRI approximation to site amplification was first introduced by Joyner *et al.* (1981) and a detailed description of the SRI method is given in Boore (2003). Only a brief summary is presented here. Given a shear-wave velocity versus depth profile $V_S(z)$ and assuming vertically incident waves, the site amplification at a particular frequency is computed as the square root of the ratio between the local seismic impedance and the seismic impedance at the source depth. The SRI site amplification is given by

$$A(f(z)) = \left(\frac{\rho_S V_S}{\bar{\rho}\,\bar{V}}\right)^{\eta}, \tag{1}$$

in which $\eta = 0.5$; ρ_S and V_S are the density and the shear-wave velocity near the source; and $\bar{\rho}$ and $\bar{V}$ are the average density and shear-wave velocity from the surface to a depth z corresponding to a quarter-wavelength for a wave with frequency f. We note that no high-frequency attenuation is included in the site amplification. The effects of damping and nonzero angles of incidence can be incorporated as multiplicative effects to the site amplification presented in equation (1). The frequency f corresponding to a depth z is given by

$$f(z) = 1/\left[4\int_0^z \frac{1}{V(z)}dz\right]. \tag{2}$$

BA23 examined the ratio of site amplification obtained from the FR method (A_{FR}) relative to that obtained with the SRI method (A_{SRI}) for a suite of eleven V_S profiles with V_{S30} ranging from 360 to 2000 m/s (see fig. 1 of BA23). A_{SRI} and A_{FR} were computed using the methods described in Boore (2013). A detailed description of this analysis is provided in BA23, and a brief description is provided here. Plots of $A_{\mathrm{FR}}/A_{\mathrm{SRI}}$ versus frequency and versus depth revealed ratios greater than 1.0 at all frequencies corresponding to depths above the half-space for the different profiles. They postulated that this observed difference in site amplification between the SRI and FR methods is due to the exponent of the ratio of seismic impedance in the SRI method ($\eta = 0.5$) compared to that of the FR method. This exponent is equal to 1.0 for a one-layer profile for the FR method and generally varies between 0.5 and 1.0 for multilayered profiles.

Based on this observation, BA23 computed the exponent $\eta = \frac{1}{2}\frac{\log(A_{\mathrm{FR}})}{\log(A_{\mathrm{SRI}})}$ required to modify the SRI method to match the FR site amplifications. Five V_S profiles deemed realistic that extended to a depth of 8 km were used to compute η: the Al Atik and Abrahamson (2021; hereafter, AAA21) V_S profile compatible with the average site response in the Chiou and Youngs (2014; hereafter, CY14) GMPM with $V_{S30} = 760$ m/s, a continuous approximation of the Kamai *et al.* (2013; hereafter, Ka13) V_S profile with $V_{S30} = 760$ m/s, and the Boore (2016; hereafter, B16) V_S profiles with $V_{S30} = 360$, 760, and 1500 m/s. The computed η and their average versus the

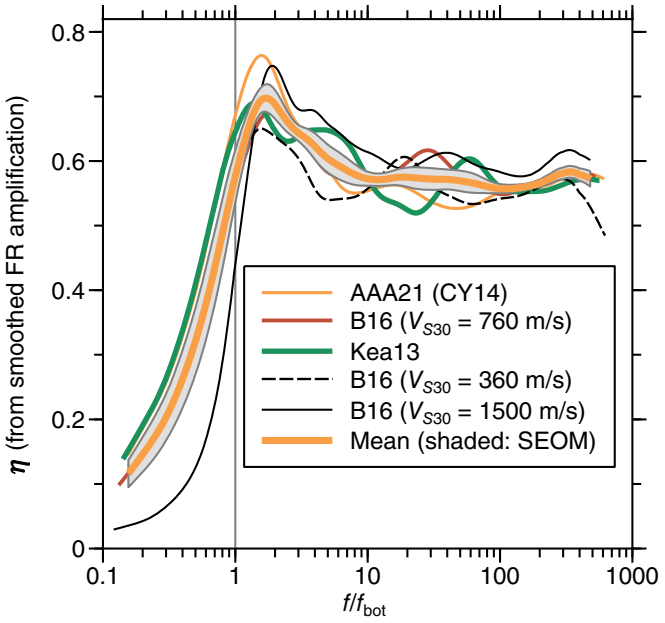

Figure 1. The computed η exponent of the square-root-impedance (SRI) method required to match the full-resonance (FR) site amplifications for the five V_S profiles considered by BA23 and their mean and standard error of the mean (SEOM) (revised fig. 10c in Boore and Abrahamson, 2023, removing the "Fit to mean" curve, which is no longer used in computing the modified SRI amplifications). The color version of this figure is available only in the electronic edition.

normalized frequency f/f_{bot}, in which f_{bot} is the quarter-wavelength frequency corresponding to the bottom of each profile are shown in Figure 1. Smoothing splines were used to smooth the FR site amplifications before computing η. The mean η values relative to f/f_{bot} were proposed for use to compute modified SRI site amplifications that better match the FR site amplifications over a wide range of frequencies.

METHODS

We followed the method of BA23 for the adjustment of the SRI site amplifications to better match those obtained from the FR method. Namely, we accepted the BA23 hypothesis that the difference between the SRI and the FR site amplifications is due to differences in the exponent η of the ratio of seismic impedances between the two methods. We investigated the frequency-dependent η for a range of V_S profiles in different V_{S30} bins and develop frequency-dependent and V_{S30}-dependent η values that can be used to modify the SRI site amplifications. For this purpose, we generated realistic V_S profiles for V_{S30} values ranging from 180 to 1500 m/s. The method for the development of V_S profiles is described in this section followed with the description of computed η.

Development of V_S profiles

A range of realistic V_S profiles was generated for each of the following V_{S30} values: 180, 200, 255, 300, 360, 400, 500, 523, 600, 700, 760, 800, 900, 1000, 1068, 1100, 1200, and 1500 m/s. These V_S profiles are characterized by a decreasing gradient of velocity with depth and a smoothly varying depth dependence without significant step changes in seismic impedance. Although an infinite number of V_S profiles can satisfy these criteria, our aim was to sample the range of realistic V_S profiles for a given V_{S30} value, examine the resulting η functions, and develop the mean and uncertainty of η.

We generated a relatively large number of V_S profiles for each of the V_{S30} values listed earlier. These profiles were generated using two power-law functions of depth and were constrained by the assigned V_{S30} value and the depth and velocity of the half-space. The V_S profile as a function of depth z is given by

$$V_S(z) = \left[\frac{V_r}{(1-p)}\left(\frac{\min(z,z_{1b})}{z_r}\right)^p\right]\left(\frac{\max(z,z_{1b})}{z_{1b}}\right)^{p_2}, \qquad (3)$$

in which the term in square brackets is the first power-law function used for depths between 0 and the breakpoint z_{1b}, and the term after the square brackets is the second power-law function used for depths greater than z_{1b}. V_r is the time-averaged velocity to depth z_r, and p is less than 1.0. Note that z_r must be less than z_{1b} for the time-averaged velocity to z_r to equal the specified value of V_r. z_{2b} and V_{2b} are the depth and shear-wave velocity of the half-space. The velocity V_{1b} at the depth z_{1b} is given by substituting that depth into the term in the square brackets in equation (3). Once that velocity is determined, p_2 is given by $p_2 = \log(V_{2b}/V_{1b})/\log(z_{2b}/z_{1b})$. Given the constraints of the assigned V_{S30} ($z_r = 0.03$ km and $V_r = V_{S30}$) and the depth and velocity of the half-space (taken as $z_{2b} = 8$ km and $V_{2b} = 3.5$ km/s in this article), equation (3) reduces to two free parameters: the exponent p of the first power-law function and the depth z_{1b} at which the two power-law functions are joined.

For each of 18 V_{S30} values listed earlier, equation (3) was used to generate V_S profiles with the exponent p ranging from 0.025 to 0.6 in increments of 0.025 and the breakpoint depth, z_{1b}, between the two power-law functions was set at values of 0.1, 0.2, 0.4, 1.0, and 2.0 km. These ranges of p and z_{1b} were chosen to allow sampling of a wide range of realistic profiles with a given V_{S30} value. Equation (3) results in a $V_S = 0$ for $z = 0$. To avoid zero velocity at the ground surface, we replaced the top layer of the profile with a 0.1-m-thick constant velocity layer for which velocity results in the same travel time obtained from equation (3) for the first layer of the profile. The resulting 120 V_S profiles generated for each V_{S30} value were further constrained to have their depths to shear-wave velocity horizons of 1.0 and 2.5 km/s ($Z_{1.0}$ and $Z_{2.5}$) fall within a reasonable range for these parameters, as described subsequently.

Basin depth constraints

The parameters $Z_{1.0}$ and $Z_{2.5}$ were first used in the Next Generation Attenuation (NGA)-West2 GMPMs to represent

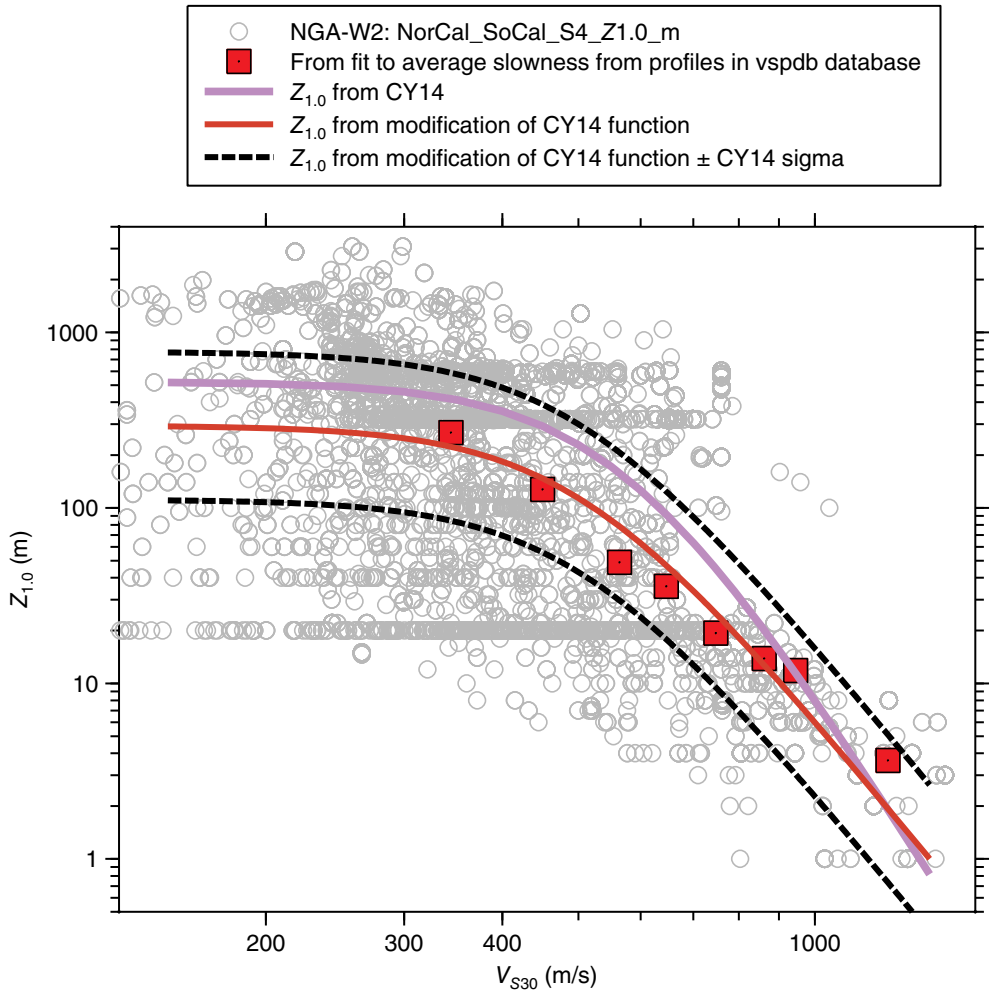

Figure 2. Estimates of $Z_{1.0}$ versus V_{S30} for sites in the Next Generation Attenuation (NGA)-West2 database. Shown are the CY14 average relationship between $Z_{1.0}$ and V_{S30}, the average $Z_{1.0}$ versus V_{S30} based on the analysis of measured V_S profiles (squares), and the approximate fit to these points given by modifying the CY14 function. The mean plus and minus sigma of the modified CY14 relationship are shown using the standard deviation of the CY14 fit (black dashed curves). The color version of this figure is available only in the electronic edition.

the thickness of near-surface sediments and to model the long-period basin response (Ancheta *et al.*, 2013). Abrahamson *et al.* (2014), Boore *et al.* (2014), and Chiou and Youngs (2014; hereafter, CY14) used the $Z_{1.0}$ parameter, whereas Campbell and Bozorgnia (2014; hereafter, CB14) used $Z_{2.5}$. For recording stations in California, the $Z_{1.0}$ and $Z_{2.5}$ depths in the NGA-West2 database (Ancheta *et al.*, 2013) were obtained by querying the 3D community velocity models (CVM) CVM-S4 (see Data and Resources) and CVM-H11 (see Data and Resources) developed by the Southern California Earthquake Center for the southern California region. Estimates of $Z_{1.0}$ and $Z_{2.5}$ were also obtained for the Bay Area region in Northern California based on version 08.3.0 of the 3D Bay Area Velocity Model described in Aagaard *et al.* (2008, 2010). Figure 2 shows the $Z_{1.0}$ estimates from the CVM-S4 model for the NGA-West2 stations in California plotted as a function of V_{S30} for V_{S30} values that are either measured or inferred based on proxies (Ancheta *et al.*, 2013). Figure 2 also shows the average $Z_{1.0}$–V_{S30} relationship developed by CY14. Similarly, CB14 developed an average $Z_{2.5}$–V_{S30} relationship for California sites in the NGA-West2 database based on the estimated $Z_{2.5}$ values.

Because most of the NGA-West2 stations have inferred V_{S30} values and inferred CVM-based estimates of basin depth parameters, we investigated the basin depths for measured V_S profiles using the shear-wave velocity profile Database (VSPDB; Ahdi *et al.*, 2018; Kwak *et al.*, 2021), which includes measured V_S profiles at locations other than seismic recording stations. A total of 1100 V_S profiles, predominantly measured in California, were downloaded from the VSPDB. These profiles varied in their total depth, and most did not extend beyond 300 m. The V_S profiles were subsequently screened to assign missing or erroneous V_{S30} values and to fix data entry issues. The profiles were then binned in V_{S30} bins ranging from 300 to 1000 m/s in 100 m/s increments and a final bin for which V_{S30} is greater than 1000 m/s. Slowness ($S = 1/V_S$) profiles were then computed, and the average slowness profile and its standard deviation were calculated for each V_{S30} bin. These average slowness profiles were then fit using the functional form $S = a + b/(z + c)$ constrained by V_{S30} to obtain the parameters a, b, and c of the smooth average slowness profiles as a function of depth z. Similarly, the standard deviation of the slowness profile was also smoothed. Figure 3 shows the slowness profiles in the V_{S30} bin of 300–400 m/s, their mean and mean plus and minus one standard deviation, and the fit to the average slowness profile.

The resulting fitted average slowness profiles for the eight V_{S30} bins are shown in Figure 4. The intersection of these profiles with a slowness of 0.001 s/m defines $Z_{1.0}$. These measured $Z_{1.0}$ values are shown with the square symbols in Figure 2 and

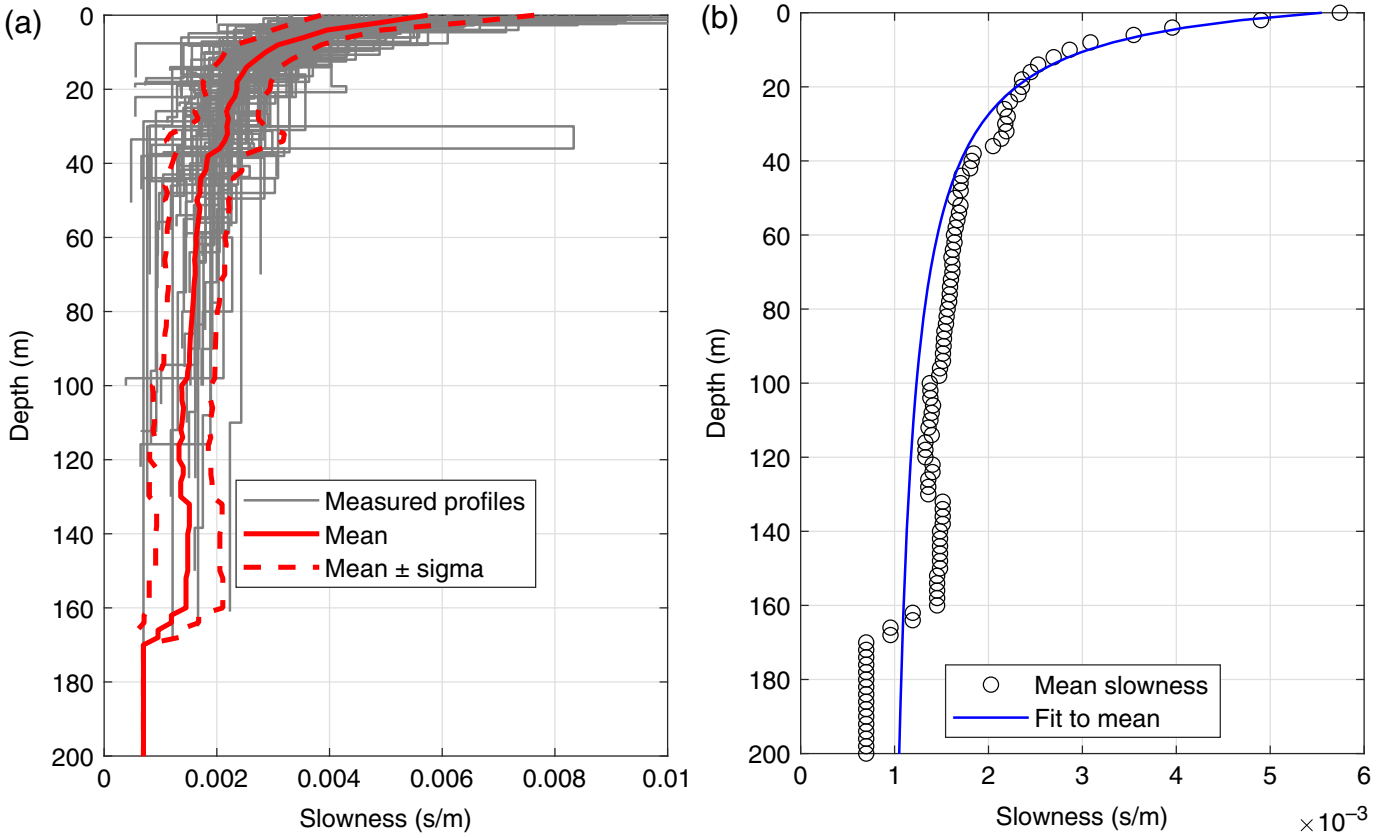

Figure 3. (a) Slowness profiles with V_{S30} between 300 and 400 m/s and their mean and mean plus and minus one standard deviation. (b) Fit to the mean slowness profile with an average V_{S30} of 344 m/s. The color version of this figure is available only in the electronic edition.

indicate that the average $Z_{1.0}$ from measured V_S profiles with V_{S30} <1000 m/s is smaller than that based on the CY14 $Z_{1.0}$ estimates derived from the CVM models. As a result, we adjusted the $Z_{1.0}$–V_{S30} relationship to follow the measured average $Z_{1.0}$ values, as shown in Figure 2.

The adjusted $Z_{1.0}$–V_{S30} relationship was used to further constrain the generated V_S profiles by imposing an acceptable range of $Z_{1.0}$ values for each V_{S30} case. Generated V_S profiles were kept if their $Z_{1.0}$ values fall within plus and minus one standard deviation of the average $Z_{1.0}$ calculated with the adjusted $Z_{1.0}$–V_{S30} relationship. The upper and lower bounds of $Z_{1.0}$ are shown in Figure 2 and use the standard deviation of $Z_{1.0}$ calculated by CY14 (Brian Chiou, written comm., 2024). Similarly, the generated V_S profiles were also screened to reject profiles with $Z_{2.5}$ values that fall outside of the plus and minus one standard deviation of the average $Z_{2.5}$–V_{S30} relationship of CB14. We note that the $Z_{2.5}$–V_{S30} relationship of CB14 was not adjusted given that the measured V_S profiles in the VSPDB database do not extend to a depth that allows for measuring $Z_{2.5}$.

The use of the $Z_{1.0}$ and $Z_{2.5}$ constraints resulted in a significant reduction of the set of V_S profiles that were used to calculate η. For example, for V_{S30} of 180 m/s, the 120 generated V_S profiles reduced to 45 acceptable profiles based on the $Z_{1.0}$ and $Z_{2.5}$ constraints. However, this reduction ensured more realistic profiles for the western United States that have a depth of sediments within the range observed in empirical data sets and community velocity models.

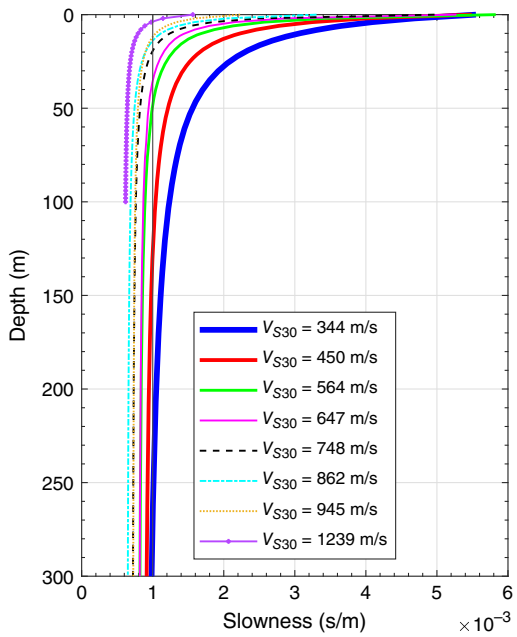

Figure 4. Average slowness profiles obtained from measured V_S profiles in the VSPDB database. The color version of this figure is available only in the electronic edition.

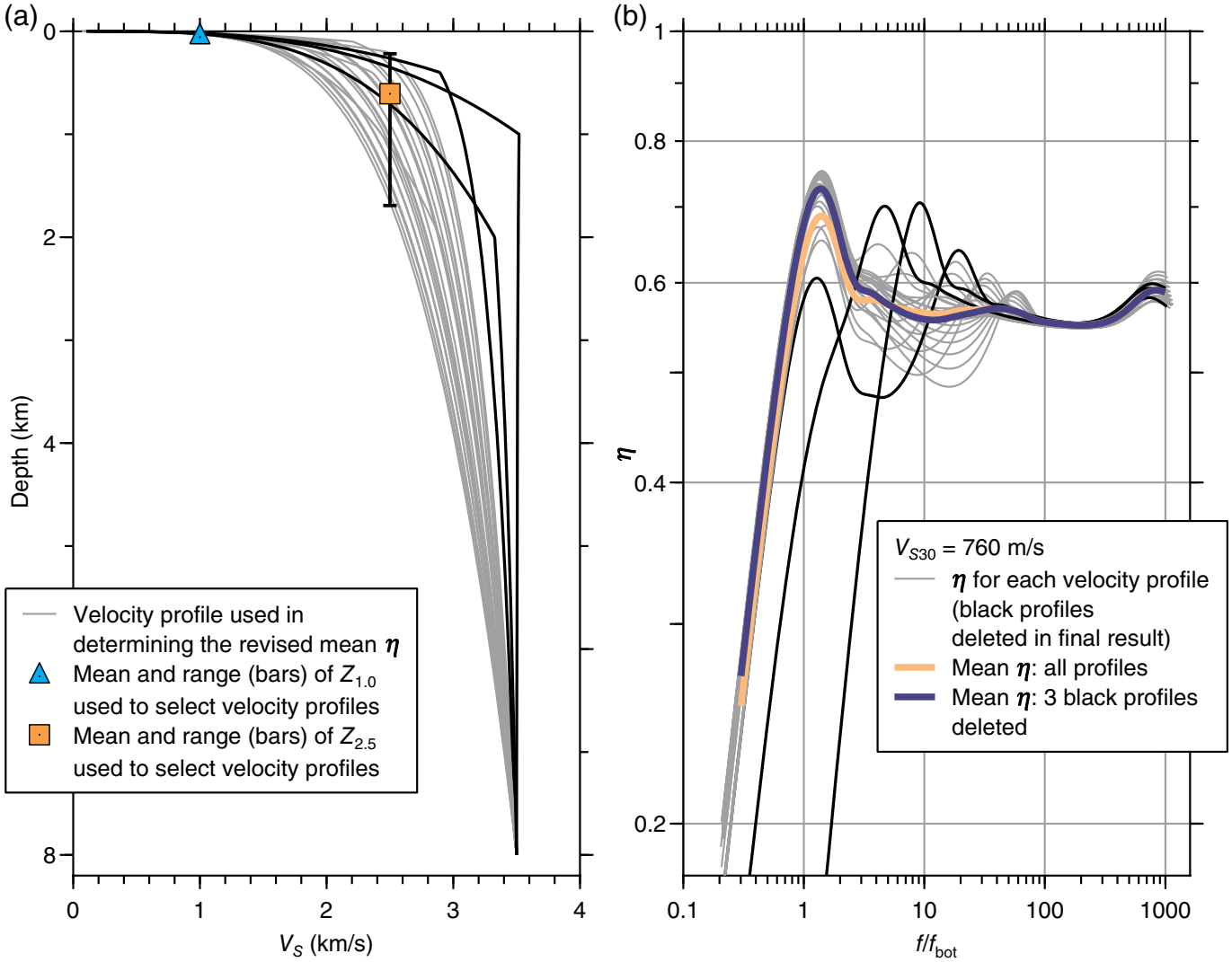

Figure 5. (a) 24 generated V_S profiles for V_{S30} of 760 m/s that satisfy the $Z_{1.0}$ and $Z_{2.5}$ constraints. (b) Corresponding exponents η. The profiles shown in black show unusual behavior in η and were discarded in the final results. The color version of this figure is available only in the electronic edition.

Computed eta (η)

For each V_S profile generated as described in the previous section, we calculated the SRI site amplification assuming zero angle of incidence, no damping, and shear-wave velocity and density at the half-space of 3.5 km/s and 2.72 g/cm^3, respectively. The density for the profiles was calculated based on the relationship between density and V_S of Boore (2016). The V_S profiles were then converted into an equivalent stack of constant-velocity layers to compute the FR site amplification. The resulting FR site amplification was calculated and the exponent η ($\eta = \frac{1}{2}\frac{\log(A_{FR})}{\log(A_{SRI})}$) was computed and smoothed using a smoothing spline algorithm.

For each V_{S30} value, the computed η as a function of normalized frequency f/f_{bot}, in which f_{bot} is the quarter-wavelength frequency corresponding to the bottom of each profile, was stacked for all the generated V_S profiles. Observations of η relative to the characteristics of the V_S profiles were noted and the average of η and its standard deviation were computed and compared to the BA23 η function. Average η functions obtained for the different V_{S30} values were compared as discussed in the next section.

RESULTS

A suite of V_S profiles and corresponding η functions were developed for each of the 18 V_{S30} values ranging from 180 to 1500 m/s following the method described in the previous section. Figure 5 shows an example of these profiles and corresponding η for V_{S30} of 760 m/s. As shown in this figure, 24 V_S profiles satisfy both the $Z_{1.0}$ and $Z_{2.5}$ ranges given the V_{S30} value. Although the η for most of the profiles shown in Figure 5 have a consistent trend and a peak for f/f_{bot} between 1 and 2, three profiles shown in black exhibit an unusual behavior compared to the rest of the profiles. These three highlighted profiles approach V_S of the half-space at a faster rate compared to the rest of the profiles, which is not consistent with our goal of using smoothly varying profiles. This results in a shift in the peak of f/f_{bot} to larger values and a reduction in average η around the peak. As a result, these

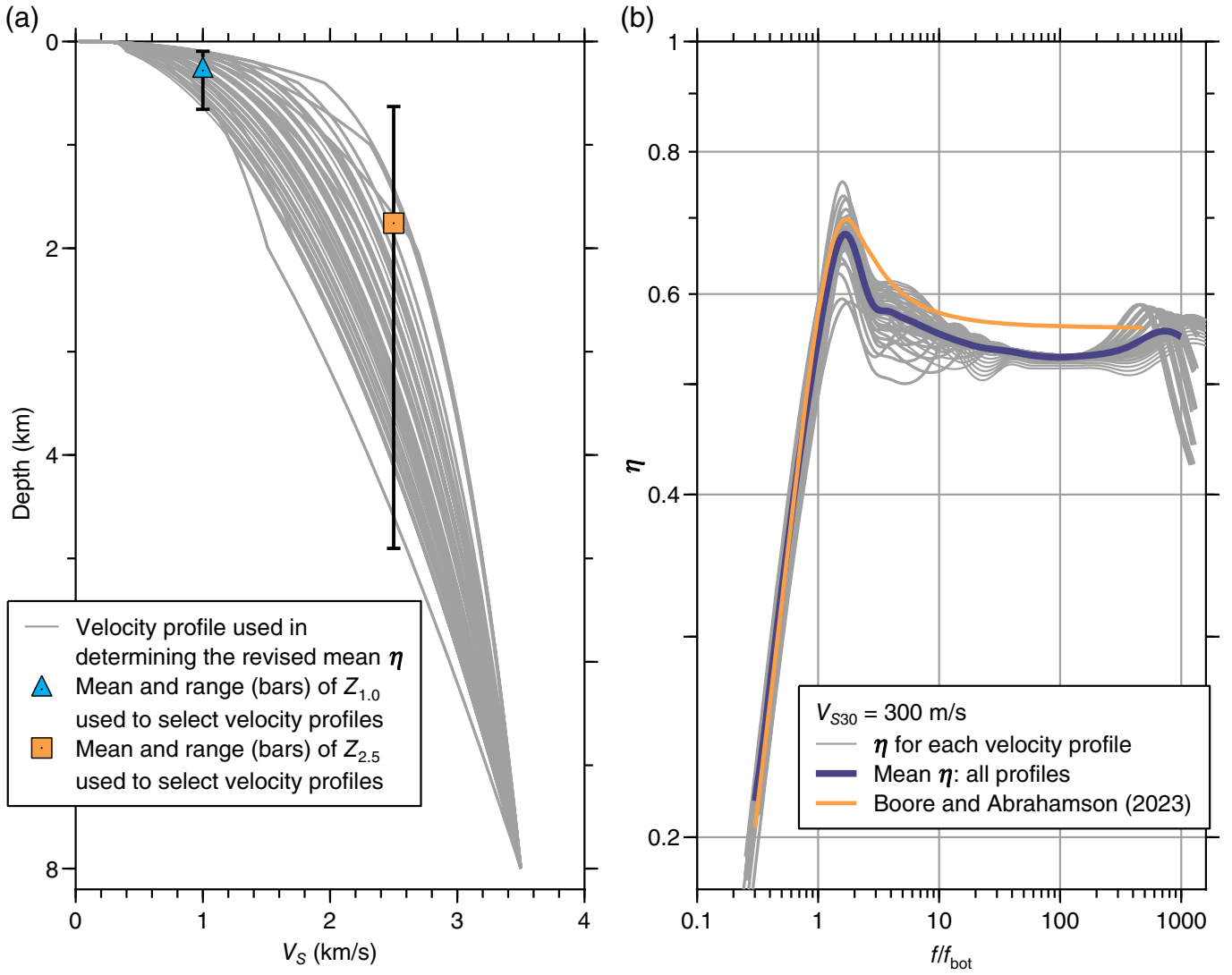

Figure 6. (a) 46 generated V_S profiles for V_{S30} of 300 m/s and (b) corresponding exponent η. The plot in panel (b) shows the average η compared to η of BA23. The color version of this figure is available only in the electronic edition.

three profiles as well as others encountered for other V_{S30} values exhibiting similar behavior were discarded from the analysis. The variability in the η functions shown in Figure 5 and the removal of profiles with unusual η behavior highlight the sensitivity of η to the details of the V_S profile.

Figure 6 shows an example of the final set of V_S profiles and corresponding η obtained for $V_{S30} = 300$ m/s. Similar plots for all 18 V_{S30} values are provided in the file PlotsOfVelocityProfilesAndEtasAllVs30Bins.pdf, in the supplemental material available to this article. The plot of η versus the normalized frequency in Figure 6 shows a consistent trend for all 46 profiles. The effects of resonance due to the first constant-velocity layer in the profiles can be seen at $f/f_{bot} > 500$ (the normalized frequencies of the resonance peaks range from 650 to 6356 for the 46 profiles shown in the figure). Resonances can also be seen at f/f_{bot} of 3–20 corresponding to the different depths z_{1b} at which the two power-law functions are joined for the different profiles and the change in the rate of the V_S profiles at this depth. The mean of η is shown in Figure 6 and compared to the BA23 V_{S30}-independent η (the 95% confidence interval is so close to the mean that it would be hard to see in the figure, so it has not been shown). The mean η obtained from this analysis for V_{S30} of 300 m/s has smaller amplitudes than the BA23 η at normalized frequencies to the right of the peak η.

A comparison of mean η obtained from this study for the 18 V_{S30} values ranging from 180 to 1500 m/s to the BA23 η is presented in Figure 7. A table of mean η and its 95% confidence interval for each V_{S30} value as a function of f/f_{bot} is provided in the supplemental material. Figure 7 indicates a clear dependence of mean η on V_{S30}. With increasing V_{S30}, the peak of the mean η shifts to smaller f/f_{bot} values closer to 1, and the amplitude of η increases. This indicates that the degree of the mismatch between the SRI and the FR site amplifications is a function of the site condition. For soft-site conditions and

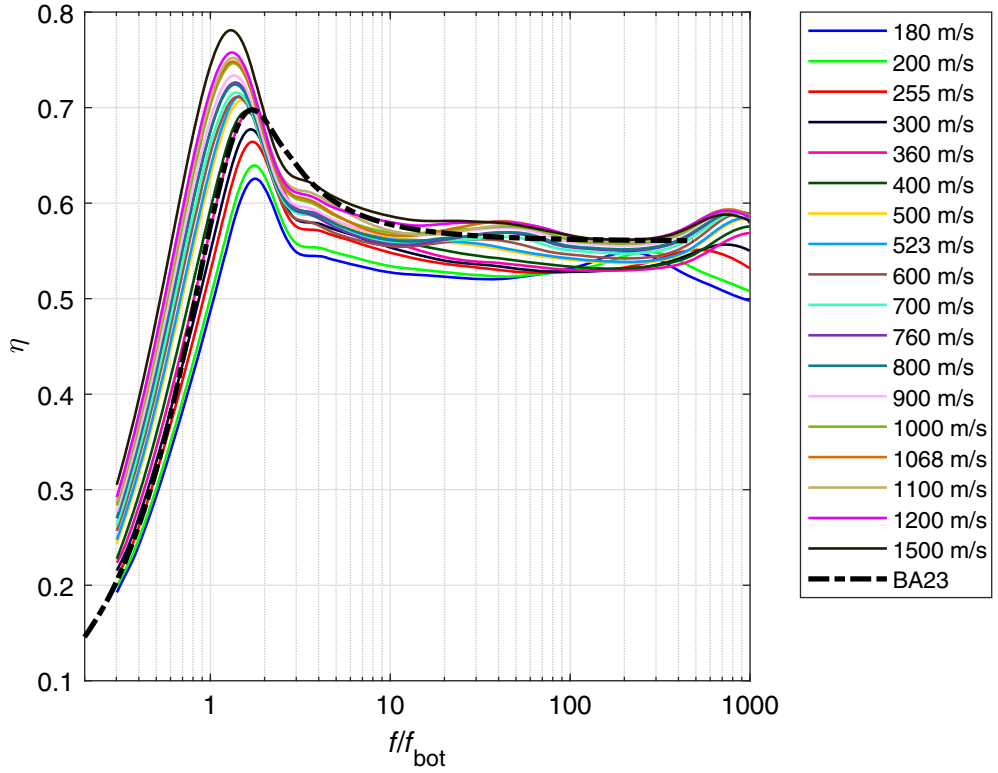

Figure 7. Mean η for V_{S30} of 180 to 1500 m/s obtained from this study compared to the BA23 η. Distinguishing between the curves on the grayscale of this figure is not important because the intent of the figure is to show the range of the V_{S30}-dependent η compared with the BA23 η. But we note that the peak values near $f/f_{bot} = 1$ increase monotonically from a low corresponding to $V_{S30} = 180$ m/s to a high for $V_{S30} = 1500$ m/s. The color version of this figure is available only in the electronic edition.

at high frequencies, the exponent η of the ratio of seismic impedances is closer to 0.5 than for the stiff site conditions. The comparison in Figure 7 indicates that using a V_{S30}-dependent η could result in a better match to the FR site amplifications compared to using the BA23 η.

DISCUSSION AND CONCLUSIONS

Given the observed dependence of η on site condition (as parameterized by V_{S30}) shown in Figure 7, the improvement in site amplification using the mean V_{S30}-dependent η obtained from this study was investigated and compared to that obtained using the V_{S30}-independent BA23 η. For the V_S profiles used in the analysis described earlier, we computed the FR site amplification and smoothed it with a cubic smoothing spline. We also computed the original SRI site amplifications ($\eta = 0.5$) and the modified SRI site amplifications (SRImod) using the BA23 η and the V_{S30}-dependent mean η derived in this study. The V_{S30}-dependent mean η's are provided in the supplemental file SummaryEtaMean95CI.csv. For application to V_{S30} values not among the 18 explicitly analyzed, mean η versus $\log(f/f_{bot})$ can be linearly interpolated to obtain the η value for the target V_{S30} value.

For each of the 18 V_{S30} values used in this study, the frequency-dependent ratios of the SRI and SRImod site amplifications relative to the FR site amplification were averaged over all V_S profiles in a bin. Example of these average site amplification ratios are shown in the bottom panel of Figure 8 for V_{S30} of 180, 760, and 1200 m/s. To avoid clutter, the variability of the amplification ratios is not shown in the figure; the one-standard-deviation band around the ratios computed using the revised η given in this article are shown in figures for each V_{S30} bin in the supplemental file PlotsOfFrAmplificationAndAmplificationRatiosAllVs30Bins.pdf. The top panel of Figure 8 shows the average FR site amplification over all profiles for V_{S30} of 180, 760, and 1200 m/s. Site amplification ratios close to 1.0 indicate a good match between the FR amplification and the SRI amplifications using the original $\eta = 0.5$ or using the modified η given either by BA23 (BA23 η) or in this article (revised η). For V_{S30} of 180, 760, and 1200 m/s, Figure 8 shows that the SRI method with $\eta = 0.5$ generally underpredicts the FR site amplifications at all frequencies, as found by Boore (2013) and Boore and Abrahamson (2023). The degree of underprediction is both frequency dependent and profile dependent. Figure 8 indicates that this underprediction is, on average, the largest for the softest site condition. For the profiles with $V_{S30} = 180$ m/s, the SRImod site amplification computed using the BA23 η shows, on average, an overprediction of the FR site amplification, which is significantly improved using the η derived in this study. For the profiles with V_{S30} of 760 and 1200 m/s, the site amplification computed using SRImod with the BA23 η match, on average, reasonably well the FR site amplifications. Using the V_{S30}-dependent η derived in this study leads to a minor average improvement in the matching of the FR site amplifications for these two site conditions. Similar comparison figures showing the improvement in average site amplification using the SRI and SRImod methods relative to the FR site amplification are included for each of the 18 V_{S30} values used in this analysis in the supplemental material.

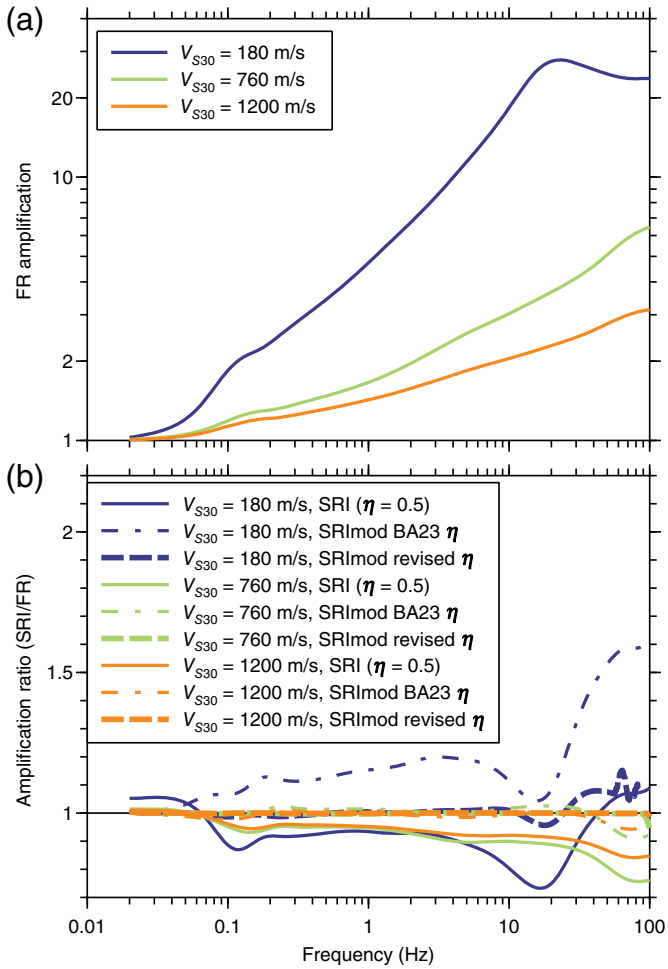

Figure 8. (a) Average FR site amplification and (b) average site amplification ratios of the SRI and SRImod methods using the BA23 η and the V_{S30}-dependent η derived in this study relative to FR for V_S profiles in the V_{S30} bins of 180, 760, and 1200 m/s used in this analysis. The color version of this figure is available only in the electronic edition.

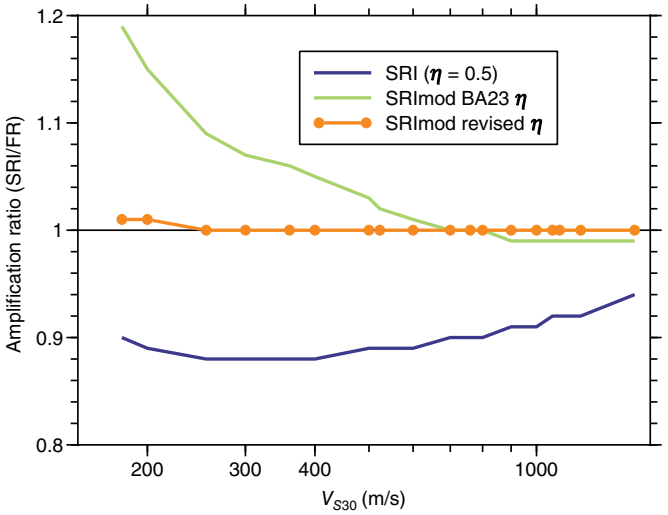

Figure 9. Average site amplification ratios versus V_{S30} of the SRI and SRImod methods using the BA23 η and the V_{S30}-dependent η derived in this study relative to FR for the V_S profiles used in this analysis. The color version of this figure is available only in the electronic edition.

To measure the overall improvement of the SRImod site amplification obtained using the V_{S30}-dependent η from this study compared to that using the BA23 η and the original SRI method, we computed the average ratio of site amplifications from the SRI and SRImod methods relative to the FR site amplification for each profile in a V_{S30} bin over the same available frequency vector greater than 0.1 Hz. These profile-dependent and frequency-independent average ratios were then averaged over all profiles in a V_{S30} bin. These average ratios are plotted in Figure 9 as a function of V_{S30} for the SRI and the SRImod site amplifications using BA23 η and the V_{S30}-dependent mean η derived in this study. This figure indicates that the average ratio of site amplification is close to 1 using η derived in this study for all V_{S30} values; this is expected because the same profiles were used to derive the V_{S30}-dependent η values. On the other hand, the SRI site amplifications consistently underpredict the FR site amplification by an average of 6%–12% over all profiles and frequencies. In addition, the SRImod site amplification obtained using BA23 η overpredicts the FR site amplification on average by up to 19% for the soft-site conditions. With increasing V_{S30}, site amplifications obtained with BA23 η closely approximate, on average, the FR site amplifications.

Given the comparisons presented in this section, we conclude that the BA23 η modification derived using only five V_S profiles generally works well for a range of V_S profiles with V_{S30} between 180 and 1500 m/s. The V_{S30}-dependent η functions derived in this study generally result in improved matches to the FR site amplification; the improvement is significant for V_{S30} less than 400 m/s and modest to negligible for the stiffer site conditions. We note that the improvement in site amplification using η derived in this study is frequency dependent and V_S profile dependent, highlighting the complexity of approximating the FR site amplification with the relatively simple SRI method and the dependence of the success of the match on the features of the V_S profile.

Finally, the analysis and observations presented in this article are applicable to gradient V_S profiles that are smoothly varying with depth and have basin depths consistent with western United States sites. We recommend the implementation of the modified SRI method using the BA23 η or the V_{S30}-dependent η derived in this study for smoothly varying gradient V_S profiles similar to those analyzed in this study. For V_S profiles that include strong impedance contrasts or that approach the half-space velocity at relatively shallow depths, site amplifications obtained with the SRI method or the modified SRI method using the BA23 η or the V_{S30}-dependent η derived in this study are unlikely to match well those obtained with the FR method. For such profiles, the FR method is more

suitable to capture resonance peaks. The uses and limitations of the SRI method compared to the FR method are further discussed in Boore (2013) for V_S profiles with and without impedance contrasts.

DATA AND RESOURCES

The database of measured V_S profiles was downloaded from the V_S-profile database (VSPDB) (https://vspdb.org/login/index.php, last accessed March 2024). For recording stations in California, the $Z_{1.0}$ and $Z_{2.5}$ depths in the Next Generation Attenuation (NGA)-West2 database (Ancheta *et al.*, 2013) were obtained by querying the 3D community velocity models (CVM) CVM-S4 (http://scec.usc.edu/scecpedia/CVM-S, last accessed September 2024) and CVM-H11 (http://scec.usc.edu/scecpedia/CVM-H, last accessed September 2024) developed by the Southern California Earthquake Center (SCEC) for the southern California region. The supplemental material includes plots for all V_{S30} bins of the velocity profiles and corresponding η values and the average of the full-resonance (FR) amplifications and the ratios of the average square-root-impedance (SRI) and FR amplifications, in which the SRI amplifications were computed using the original η (0.5) and the V_{S30}-independent (BA23) and V_{S30}-dependent (this article) η's.

DECLARATION OF COMPETING INTERESTS

The authors acknowledge that there are no conflicts of interest recorded.

ACKNOWLEDGMENTS

The authors thank Grace Parker, John Douglas, Ben Edwards, and Steve Day for constructive comments that improved the article. Any use of trade, firm, or product names is for descriptive purposes only and does not imply endorsement by the U.S. Government.

REFERENCES

Aagaard, B. T., T. M. Brocher, D. Dolenc, D. Dreger, R. W. Graves, S. Harmsen, S. Hartzell, S. Larsen, K. McCandless, S. Nilsson, *et al.* (2008). Ground motion modeling of the 1906 San Francisco earthquake II: Ground motion estimates for the 1906 earthquake and scenario events, *Bull. Seismol. Soc. Am.* **98,** 1012–1046.

Aagaard, B. T., R. W. Graves, A. Rodgers, T. M. Brocher, R. W. Simpson, D. Dreger, N. A. Petersson, S. C. Larsen, S. Ma, and R. C. Jachens (2010). Ground-motion modeling of Hayward fault scenario earthquakes, part II: Simulation of long-period and broadband ground motions, *Bull. Seismol. Soc. Am.* **100,** 2945–2977.

Abrahamson, N. A., W. J. Silva, and R. Kamai (2014). Summary of the ASK14 ground motion relation for active crustal regions, *Earthq. Spectra* **30,** 1025–1055.

Ahdi, S. K., S. Sadiq, O. Ilhan, Y. Bozorgnia, Y. M. Hashash, D. Y. Kwak, D. Park, A. Yong, and J. P. Stewart (2018). Development of a United States community shear wave velocity profile database, in *Geotechnical Earthquake Engineering and Soil Dynamics V*, American Society of Civil Engineers, Reston, Virginia, 330–339.

Al Atik, L., and N. Abrahamson (2021). A methodology for the development of 1D reference V_S profiles compatible with ground-motion prediction equations: Application to NGA-West2 GMPEs, *Bull. Seismol. Soc. Am.* **111,** 1765–1783.

Ancheta, T. D., R. B. Darragh, J. P. Stewart, E. Seyhan, W. J. Silva, B. S. Chiou, K. E. Wooddell, R. W. Graves, A. R. Kottke, D. M. Boore, *et al.* (2013). PEER NGA-West2 database, *PEER Rept. 2013/03*, Pacific Earthquake Engineering Research Center.

Boore, D. M. (2003). Simulation of ground motion using the stochastic method, *Pure Appl. Geophys.* **160,** 635–676.

Boore, D. M. (2013). The uses and limitations of the square-root impedance method for computing site amplification, *Bull. Seismol. Soc. Am.* **103**, 2356–2368.

Boore, D. M. (2016). Determining generic velocity and density profiles for crustal amplification calculations, with an update of the Boore and Joyner (1997) generic site amplification for $V = 760$ m/s, *Bull. Seismol. Soc. Am.* **106,** 316–320.

Boore, D. M., and N. Abrahamson (2023). On the ratio of full-resonance to square-root-impedance amplifications for shear-wave velocity profiles that are a continuous function of depth, *Bull. Seismol. Soc. Am.* **113,** 1192–1207.

Boore, D. M., J. P. Stewart, E. Seyhan, and G. M. Atkinson (2014). NGA-West2 equations for predicting PGA, PGV, and 5% damped PSA for shallow crustal earthquakes, *Earthq. Spectra* **30,** 1057–1085.

Campbell, K. W., and Y. Bozorgnia (2014). NGA-West2 ground motion model for the average horizontal components of PGA, PGV, and 5% damped linear acceleration response spectra, *Earthq. Spectra* **30,** 1087–1115.

Chiou, B. S.-J., and R. R. Youngs (2014). Update of the Chiou and Youngs NGA model for the average horizontal component of peak ground motion and response spectra, *Earthq. Spectra* **30,** 1117–1153.

Joyner, W. B., R. E. Warrick, and T. E. Fumal (1981). The effect of Quaternary alluvium on strong ground motion in the Coyote Lake, California, earthquake of 1979, *Bull. Seismol. Soc. Am.* **71,** 1333–1349.

Kamai, R., N. Abrahamson, and W. Silva (2013). Nonlinear horizontal site response for the NGA-West2 project, *PEER Report No. 2013/12*, Pacific Earthquake Engineering Research Center.

Kwak, D. Y., S. K. Ahdi, P. Wang, P. Zimmaro, S. J. Brandenberg, and J. P. Stewart (2021). Web portal for shear wave velocity and HVSR databases in support of site response research and applications, *UCLA Geotechnical Engineering Group*, doi: 10.21222/C27H0V.

Phung, V-B., and N. Abrahamson (2024). Methodology for developing empirical ground-motion models with compatible shear-wave profiles and kappa values, *Bull. Seismol. Soc. Am.* (under review).

Manuscript received 13 June 2024
Published online 27 September 2024